Molecular Crystals and Liquid Crystals

Publication details, including instructions for authors and subscription information:
http://www.tandfonline.com/loi/gmcl20

Optimization of Polymer Stabilization Condition of Bend Alignment in Pi-cell

Youichi Asakawa [a], Naoki Takatuka [a], Taiju Takahashi [a] & Susumu Saito [a]

[a] Department of Electronic Engineering, Kogakuin University, Nakano-cho Hachioji-shi, Tokyo, Japan

Version of record first published: 22 Sep 2010

To cite this article: Youichi Asakawa, Naoki Takatuka, Taiju Takahashi & Susumu Saito (2007): Optimization of Polymer Stabilization Condition of Bend Alignment in Pi-cell, Molecular Crystals and Liquid Crystals, 476:1, 43/[289]-59/[305]

To link to this article: http://dx.doi.org/10.1080/15421400701733868

Mol. Cryst. Liq. Cryst., Vol. 476, pp. 43/[289]–59/[305], 2007

ISSN: 1542-1406 print/1563-5287 online
DOI: 10.1080/15421400701733868

Optimization of Polymer Stabilization Condition of Bend Alignment in Pi-cell

Youichi Asakawa
Naoki Takatuka
Taiju Takahashi
Susumu Saito
Department of Electronic Engineering, Kogakuin University, Nakano-cho Hachioji-shi, Tokyo, Japan

Director profiles and electrooptical properties in polymer-stabilized π cells used in optically compensated bend (OCB) liquid crystal displays (LCDs) are theoretically investigated by introducing an additional term which expresses the effect of polymer stabilization on the free energy density. The conditions required to stabilize the bend alignment definitively have been theoretically clarified and experimentally confirmed. As a result, the bend alignment is successfully stabilized even if the twist state is more stable than the bend state before the application of polymer-stabilization treatment.

Keywords: bend alignment; nematic liquid crystal; OCB-LCD; polymer stabilization; UV curable liquid crystalline monomers

1. INTRODUCTION

The optically compensated bend (OCB) nematic liquid crystal display (LCD) has attracted much attention due to its superior characteristics such as a fast response time and a wide viewing angle [1,2]. In the OCB-type LCD, the π cell is used with an optical compensation film. The π cell is constructed using a pair of substrates which are rubbed in parallel directions. The OCB-type LCD has one serious drawback

We express our most sincere thanks to Dr. Nakanowatari of Merck Co., Ltd. for his kind support in supplying UV curable liquid crystalline monomers, and to Mr. Niikura for his cooperation in these experiments.

This work was supported by MEXT. HAITEKU(2005).

Address correspondence to Susumu Saito, Department of Electronic Engineering, Kogakuin University, 2665-1 Nakano-cho Hachioji-shi, Tokyo 192-0015, Japan. E-mail: cd05001@ns.kogakuin.ac.jp

in that it needs the initialing operation in which molecular alignment is made to undergo transition from splay to bend alignment by applying a high voltage at start-up, and always needs an operating voltage higher than its critical voltage to maintain the bend alignment.

To mitigate this problem, the following methods have been proposed. The first method is to complete the transition from splay alignment to bend alignment quickly by applying a high voltage [3] and by forming transition nuclei on the substrate surfaces [4,5]. However, this method does not effectively solve the problem, because the initial voltage application is still needed. The other method, which aims to make the initial voltage application unnecessary, involves polymer stabilization of the bend alignment by the formation of a polymer network [6,7] or an aligned polymer wall [8] using the optical polymerization of UV curable liquid crystalline monomers or reactive mesogen molecules dissolved within the liquid crystal host. This method is an effective means of solving the problem of the OCB-type LCD.

Uchida et al. first attempted this method to stabilize the bend alignment in the π cell [6]. However, it has been recognized that they could only stabilize the twist state but not the bend state. Recently, Kim and Chen successfully stabilized the bend state by experimentally optimizing the concentration of reactive mesogen and the irradiation energy of UV light and by observing in detail the morphology of the polymer network by scanning electron microscopy [7].

Although many experimental results concerning polymer stabilization for nematic liquid crystal cells have been reported, a theoretical investigation has not been reported except in theoretical considerations made by Kossyrev et al. [9] concerning the Freedericksz transition.

Takahashi et al. reported a theoretical simulation for polymer-stabilized ferroelectric liquid crystals [10]. In their report, they introduced the additional term for free energy density to express the effect of polymer stabilization.

In this report, the conditions required to stabilize the bend alignment definitively are investigated theoretically by applying the method proposed by Takahashi et al. to the case of nematic liquid crystals, after which, the theoretically simulated results are compared with the experimental results.

2. THEORETICAL FRAMEWORK

2.1. Material Equations

Based on the liquid crystal continuum theory by Frank and Oseen, elastic free energy density F_{elas} and dielectric free energy density F_{diel}

are given by

$$F_{elas} = \frac{1}{2}K_{11}(div\mathbf{n})^2 + \frac{1}{2}K_{22}(\mathbf{n}\cdot rot\mathbf{n})^2 + \frac{1}{2}K_{33}(\mathbf{n}\times rot\mathbf{n})^2, \quad (1)$$

$$F_{diel} = \frac{1}{2}\varepsilon_0\varepsilon \boldsymbol{E}\bullet \boldsymbol{E}, \quad (2)$$

where $\mathbf{n}$ is the director vector, $\boldsymbol{E}$ is the electric field vector, ε is the relative dielectric tensor, ε_0 is the vacuum dielectric constant, and K_{11}, K_{22}, and K_{33} are elastic constants for splay, twist, and bend deformations, respectively.

An additional term F_{stab} shown in Eq. (3) which represents the contribution of polymer stabilization to the free energy density F of liquid crystal bulk is introduced in addition to the sum of F_{elas} and F_{diel}

$$F_{stab} = \frac{1}{2}A_{stab}[1 - (\mathbf{n}_{stab}\bullet \mathbf{n})^2], \quad (3)$$

where A_{stab} is the polymer stabilization coefficient, and $\mathbf{n}_{stab}$ represents the director profile when the polymer stabilization is carried out. The expression is similar to that first introduced by Takahashi et al. for a polymer-stabilized ferroelectric liquid crystal cell. It is thought that the polymer stabilization coefficient A_{stab} depends on the density of the polymer chain generated by a photopolymerization reaction induced by UV light irradiation and on the manner of interaction between the polymer chain and liquid crystal molecules.

The total free energy density is given by

$$F = F_{elas} + F_{stab} + F_{diel}. \quad (4)$$

In this analysis, one-dimensional approximation is assumed. That is, it is assumed that the director profile varies only along the normal direction, defined as the z axis, of the substrate surfaces.

Equations (1) to (3) can be rewritten as follows with respect to this model,

$$\begin{aligned} F_{elas} = {} & \frac{1}{2}K_{11}(\partial_z n_Z)^2 + \frac{1}{2}\{K_{33} + (K_{22} - K_{33})n_y^2\}(\partial_z n_x)^2 \\ & + \frac{1}{2}\{K_{33} + (K_{22} - K_{33})n_x^2\}(\partial_z n_y)^2 \\ & - (K_{22} - K_{33})n_x n_y(\partial_z n_x)(\partial_z n_y), \end{aligned} \quad (5)$$

$$F_{stab} = \frac{1}{2}A_{stab}[1 + (n_{stabx}\ n_x + n_{staby}\ n_y + n_{stabz}\ n_z)^2], \quad (6)$$

$$F_{diel} = \frac{1}{2} D_z^2 \, \varepsilon_0^{-1} (\varepsilon_n + \Delta\varepsilon n_z^2)^{-1}. \tag{7}$$

We assume the Rapini-Papoular potential as follows for the surface energy density.

$$\begin{aligned} F^S(l) &= \frac{1}{2} C_{\theta_l} \sin^2(\theta(l) - \theta_l) + \frac{1}{2} C_{\phi l} \sin^2(\Delta\varphi(l)) \\ &= \frac{1}{2} C_{\theta l} [1 - (\mathbf{n}_l \bullet \mathbf{n}'(l))^2] + \frac{1}{2} C_{\phi l} [1 - (\mathbf{n}_{l_0} \bullet \mathbf{n}(l)_0)^2], \end{aligned} \tag{8}$$

where $l = 0$ for the interface at z = 0, $l =$ d for the interface at z = d, and $\mathbf{n}_l$ and $\mathbf{n}(l)$ represent the unit vector parallel to the easy axis and the director vector at the interface, respectively. The coefficients $C_{\theta l}$ and $C_{\phi l}$ are the polar anchoring energy and the azimuthal anchoring energy, respectively; $\mathbf{n}'(l)$ is the unit vector obtained by rotating $\mathbf{n}(l)$ to the plane which includes $\mathbf{n}_l$ and is perpendicular to the x-y planewith respect to the z axis. Furthermore, $\mathbf{n}_{l0}$ and $\mathbf{n}(l)_0$ are the unit vectors with projections of $\mathbf{n}_l$ and $\mathbf{n}(l)$ onto the substrate surfaces, respectively.

Rewriting Eq. (8) with respect to the present model, one obtains the following equations:

$$\begin{aligned} F^S(l) = \frac{1}{2} C_{\theta l} \left[1 - \left\{ \sqrt{n_x(l)^2 + n_y(l)^2} (n_{lx} \cos\phi_l + n_{ly} \sin\phi_l) + n_{lz} n_z(l) \right\}^2 \right] \\ + \frac{1}{2} C_{\phi l} \left[1 - \frac{1}{(n_{lx}^2 + n_{l_y}^2)(n_x(l)^2 + n_y(l)^2)} \{ n_{lx} n_x(l) + n_{ly} n_y(l) \}^2 \right]. \end{aligned} \tag{9}$$

2.2. Differential Equations to be Solved to Obtain Director Profiles

The momentum balance equations for the LC bulk and the interfaces at z = 0 and d are to be solved. When the momentum balance equations are solved with respect to the tilt angle θ and azimuthal angle ϕ, the points at which ϕ takes the value of $\pi/2$ and either θ or ϕ varies discontinuously become singularity points. To avoid such singularity, a particular technique must be used [11]. We solved the momentum balance equations with respect to three components n_x, n_y, and n_z of $\mathbf{n}$, because we could get true solutions even at the singularity points without special procedures. It is easy to obtain the solutions with respect to θ and ϕ from n_x, n_y, and n_z. In this study, the rotational viscous torque and the surface anchoring effect are taken into account, but for simplicity, the flow effect and the surface dissipation are

ignored. As a result, the following simultaneous nonlinear equations are obtained. For the LC bulk

$$\frac{\partial F}{\partial n_x} - \partial_z \frac{\partial F}{\partial(\partial_z n_x)} + \lambda_L n_x + \gamma_1 \frac{\partial n_x}{\partial t} = 0 \tag{10}$$

$$\frac{\partial F}{\partial n_y} - \partial_z \frac{\partial F}{\partial(\partial_z n_y)} + \lambda_L n_y + \gamma_1 \frac{\partial n_y}{\partial t} = 0 \tag{11}$$

$$n_x^2 + n_y^2 + n_z^2 = 1 \tag{12}$$

where γ_1 is the rotational viscous coefficient and λ_{L} a Lagrange multiplier.

For the surfaces at z = 0

$$\frac{\partial F^{\mathrm{s}}(0)}{\partial n_x(0)} - \frac{\partial F}{\partial(\partial_z n_x)}\Big|_{z=0} = 0 \tag{13}$$

$$\frac{\partial F^{\mathrm{s}}(0)}{\partial n_y(0)} - \frac{\partial F}{\partial(\partial_z n_y)}\Big|_{z=0} = 0 \tag{14}$$

$$n_x(0)^2 + n_y(0)^2 + n_z(0)^2 = 1 \tag{15}$$

For the surface at z = d

$$\frac{\partial F^{\mathrm{s}}(d)}{\partial n_x(d)} + \frac{\partial F}{\partial(\partial_z n_x)}\Big|_{z=d} = 0 \tag{16}$$

$$\frac{\partial F^{\mathrm{s}}(d)}{\partial n_y(d)} + \frac{\partial F}{\partial(\partial_z n_y)}\Big|_{z=d} = 0 \tag{17}$$

$$n_x(d)^2 + n_y(d)^2 + n_z(d)^2 = 1 \tag{18}$$

Detailed expressions of each terms in the eqs. (10), (11), (13), (14), (16) and (17) for this model are shown in the Appendix.

2.3. Method of Numerical Calculation

To solve the nonlinear simultaneous differential equations consisting of Eqs. (10)–(18), we divided the interval [0, d] into 100 subintervals and rewrote the equations in terms of differences. The simultaneous equations for the resultant 303 elements were numerically solved by Newton's method.

Considering that

$$\sum_i n_i \frac{\partial n_i}{\partial t} = \frac{1}{2} \frac{\partial \sum_i n_i n_i}{\partial t} = 0 \tag{19}$$

the Lagrange multiplier is determined by

$$\lambda_L = -\sum_i n_i \left[\frac{\partial F}{\partial n_i} - \partial_z \frac{\partial F}{\partial (\partial_z n_i)} \right]. \tag{20}$$

The notation $\sum_i$ means the sum with respect to x, y and z.

To investigate the changes in the director profile with the increase or decrease in applied voltage, the applied voltage V was linearly varied with time. A sufficiently slow rate of variation for example 0.5 V/min, was assumed to obtain a solution as near as possible to the steady state.

3. THEORETICAL CONSIDERATION

3.1. Gibbs Free Energy for the Splay, Bend, and Twist Alignments Before Polymer Stabilization

3.1.1. Calculation of the Gibbs Energy

The Gibbs energy GE are calculated from

$$GE = \int_0^d (F_{elas} - F_{diel}) dz. \tag{21}$$

Explicit expressions for F_{elas} and F_{diel} are given by Eq. (5) and Eq. (7), respectively. When no voltage is applied, it is assumed that $F_{diel} = 0$.

3.1.2. When No Voltage is Applied

In Figure 1 the Gibbs free energy calculated as a function of pretilt angle θ_0 is plotted for the case of no voltage application. In these calculations, it was assumed that $F_{diel} = 0$ and $F_{stab} = 0$, that is, $V = 0$ and $A_{stab} = 0$. The parameters of the liquid crystal used in the calculation are listed for nematic liquid crystal ZLI-2293 in Table 1. For the cell gap, $d = 6\,\mu m$ was assumed.

When the pretilt angle is lower than θ_2, as is shown in the figure, the splay alignment is the stable state since it has the lowest Gibbs free energy among the splay, bend, and twist states. Conversely, when the pretilt angle is higher than θ_2, the bend state is the stable state since it has the lowest Gibbs free energy of the three states.

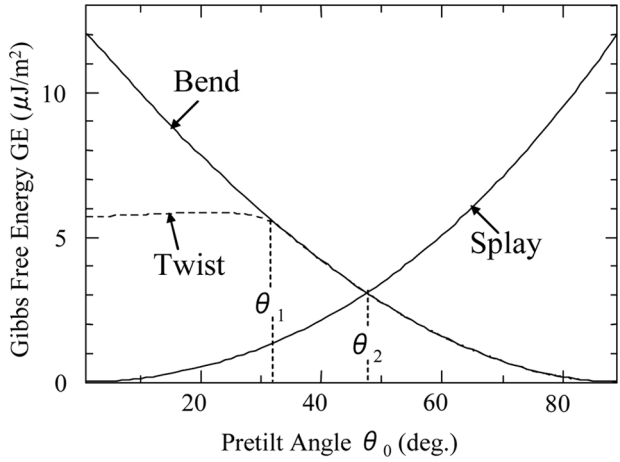

FIGURE 1 Gibbs free energy for splay, bend and twist states of alignment under the condition of no voltage application.

When the pretilt angle is lower than θ_1, the twist alignment has a lower Gibbs free energy than the bend alignment. However, when the pretilt angle is higher than θ_1, the bend alignment and the twist alignment degenerate as shown in Figure 2. The angle θ_1 depends strongly on the twist elastic constant K_{22}. For common nematic liquid crystals which are commercially available, the angle θ_1 is in the range of 25 to 35°. The pretilt angle obtained by the rubbing method using the polyimide alignment material is lower than θ_1, which is in the upper range. Thus, the twist alignment is in a lower metastable state than that of the bend alignment.

3.1.3. When Voltage is Applied

Figure 3 shows the calculated results for the relationships between the applied voltage and the Gibbs free energy for the splay, twist and bend states of alignment. In these calculations, it was assumed that $F_{stab} = 0$, that is, $A_{stab} = 0$. Moreover, it was assumed that pretilt angle is 5°. The parameters of the liquid crystal used in the calculation are listed for nematic liquid crystal ZLI-2293 in Table 1.

TABLE 1 Parameter Used in Our Calculations

$K_{11} = 12.5 \times 10^{-12}$ N	$n_e = 1.63$
$K_{22} = 7.3 \times 10^{-12}$N	$n_o = 1.50$
$K_{33} = 17.9 \times 10^{-12}$N	$\gamma_1 = 149$ mPas
$\varepsilon_p = 14.1$	$d = 6.0\,\mu$m
$\varepsilon_n = 4.1$	$\lambda = 550$ nm

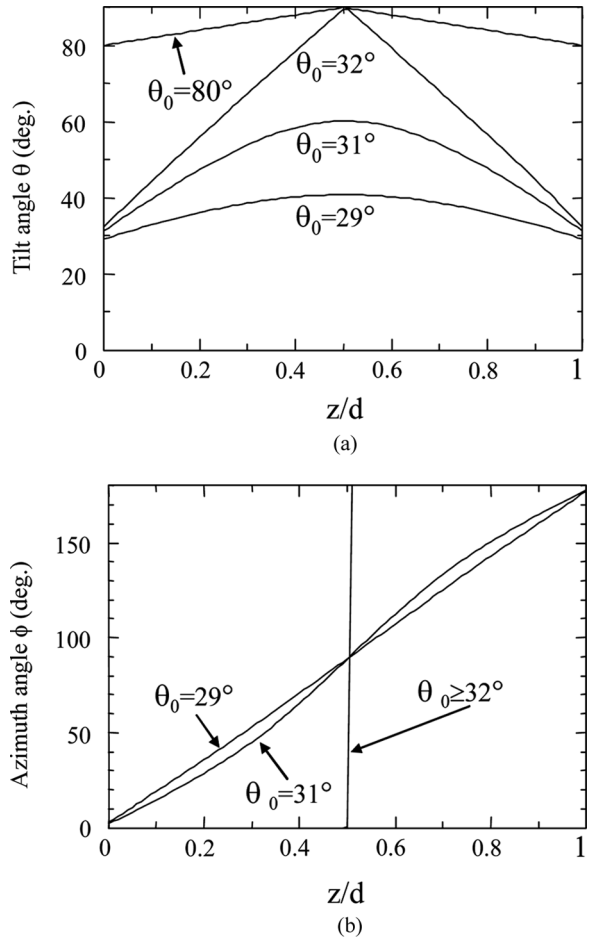

FIGURE 2 Dependence of director profiles on pretilt angle, θ_0, in 180° twist alignment: (a) tilt angle and (b) azimuth angle.

When no voltage is applied, the splay state has the lowest Gibbs free energy. Thus, the splay state is realized as the initial equilibrium state. When the applied voltage V is increased to over the voltage V_C, the configuration of molecular alignment changes to the bend state or the twist state from the splay state, since the Gibbs energy of the splay state become higher than the energies of the bend and twist states. If the applied voltage is decreased from a voltage higher than V_C, the configuration of molecular alignment takes the states of bend or twist within the range $V_C > V > V_{C1}$, and it takes the twist

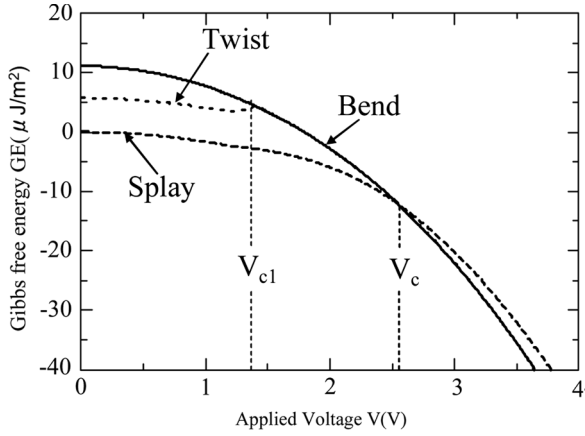

FIGURE 3 Relationship between applied voltage and Gibbs free energy for splay, bend and twist states of alignment.

state in the range $V < V_{C1}$. The twist state finally relaxes to the splay state.

3.2. Simulation for Director Profile After Polymer Stabilization

3.2.1. Procedure of the Calculation

The procedure for this simulation was conducted as follows. It was assumed that the initial configuration of the molecules was in the 180° twist state. Presuming that the voltage was increased from 0 V to V_{stab} at a constant rate, the director profiles were calculated for each time interval under the condition $A_{stab} = 0$. The voltage V_{stab} is selected to be in a range in which the center tilt angle is $\pi/2$. When the center tilt angle becomes $\pi/2$ the twist state transforms to the bend state. The director profile at $V = V_{stab}$ was memorized as the profile of $\mathbf{n}_{stab}$. Then assuming the appropriate value for A_{stab}, the applied voltage was decreased to 0 V at a constant rate. In this process, the director profile was also calculated for each time interval.

3.2.2. Simulated Results and Discussion

The parameters of the liquid crystal used in these calculations are listed for nematic liquid crystal ZLI-2293 in Table 1, and the pretilt angle is assumed to be 5°.

The dotted line in Figure 4 shows the director profiles of $\mathbf{n}_{stab}$ calculated for $V_{stab} = 10.0$ V, and the solid line shows the director profiles resulting from the polymer stabilization for some values of A_{stab} when

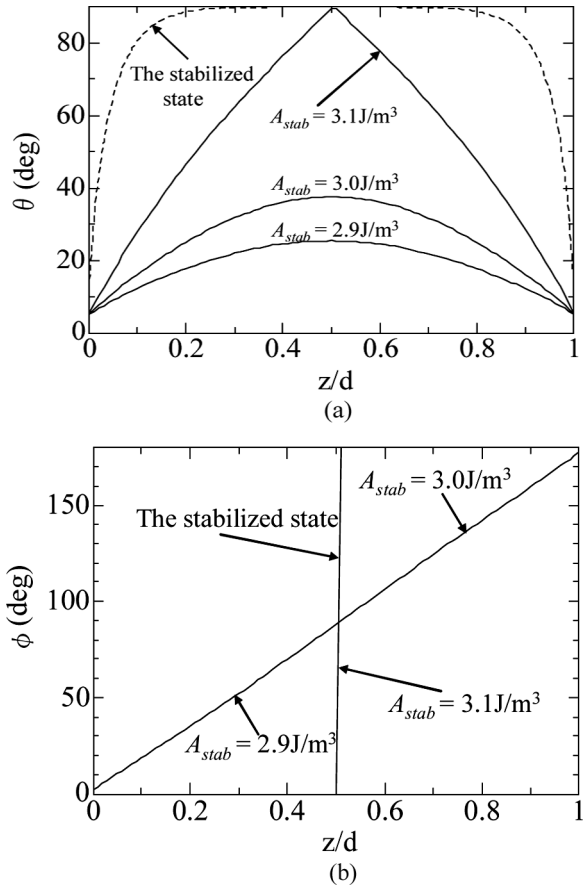

FIGURE 4 Dependence of director profiles on polymer stabilization coefficient, A_{stab}, resulting from polymer stabilization treatment in bend alignment under application of $V_{stab} = 10\,V$. (a) tilt angle and (b) azimuth angle.

no voltage is applied. Figures 4(a) and 4(b) show the profiles of the tilt angle and the azimuth angle, respectively. The tilt angle profile corresponding to the $\mathbf{n}_{stab}$ takes $\pi/2$ at $z = d/2$, and the azimuth angle profile of $\mathbf{n}_{stab}$ varies discontinuously at $z = d/2$ from 0 to π. This means that the polymer-stabilizing treatment was applied to the bend alignment. The director profiles resulting from the polymer stabilization for A_{stab} larger than the critical value $A_{stabc} = 3.1\,J/m^3$ are apparently in the bend alignment, since in this case, the tilt angle is $\pi/2$ at $z = d/2$, and the azimuth angle changes discontinuously from 0 to π at $= d/2$. When A_{stab} is smaller than A_{stabc}, however, the director profile

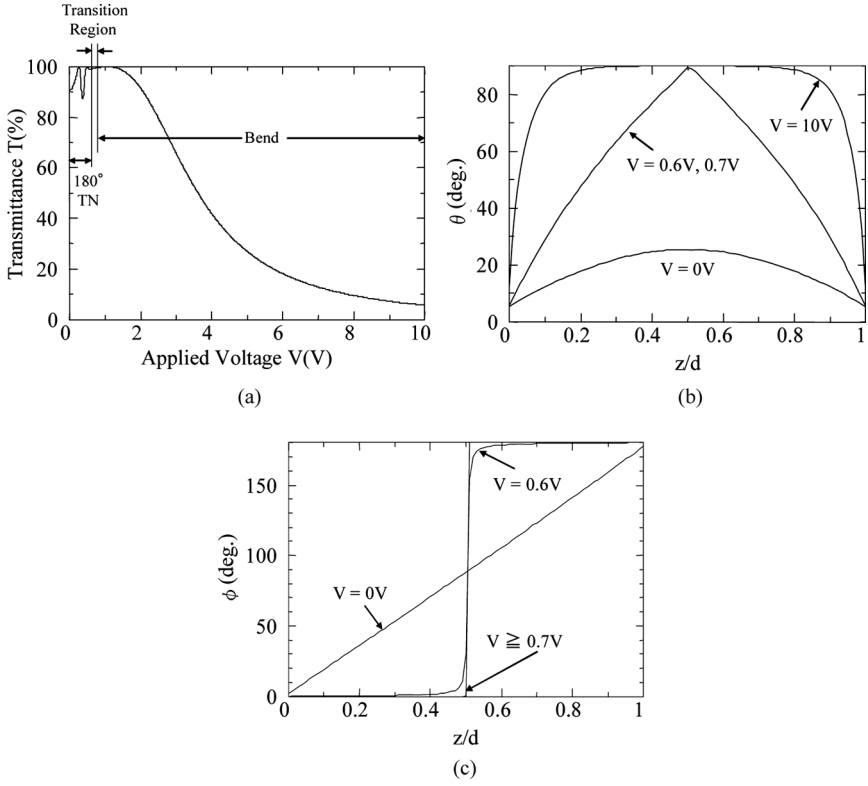

FIGURE 5 V-T curves and director profiles at each voltage when A_{stab} is $2.9\,J/m^3$: (a) V-T curve, (b) tilt angle, (c) azimuth angle.

resulting from the polymer stabilization is in the twist state, because the center tilt angle is lower than $\pi/2$ and the azimuth angle changes continuously from zero to 180° along the z direction.

In Figure 5(a), the V vs T relation is calculated for the change of director profiles, which are shown in Figures 5(b) and 5(c). In these calculations, it was assumed that polymer stabilization was carried out under conditions where $V_{stab} = 10\,V$ and $A_{stab} = 2.9\,J/m^3$. As can be seen, when $V = 0\,V$, the director profile is in the twist alignment. When the applied voltage is increased from 0 V, the director profile transforms to the bend state above $V = 0.7\,V$, because the center tilt angle becomes $\pi/2$ and the azimuth angle changes discontinuously at $z = d/2$. When the director profile is in the twist state below $V = 0.7\,V$, the transmittance varies characteristically in the voltage range as shown in Figure 5(a). However, when A_{stab} is larger than

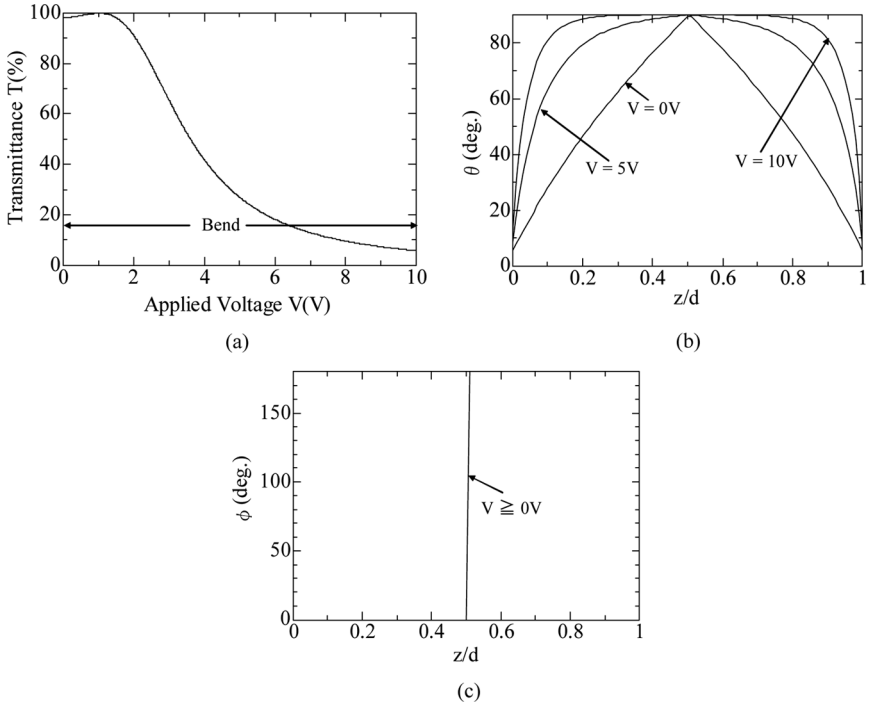

FIGURE 6 V-T curves and director profiles at each voltage when A_{stab} is $3.1\,J/m^3$: (a) V-T curves, (b) tilt angle, (c) azimuth angle.

$3.1\,J/m^3$, the director profile adopts the bend alignment over all the voltage range and the transmittance varies with the increase in applied voltage as shown in Figure 6(a). It should be noted that A_{stab} must be larger than the critical value A_{stabc} to confidently obtain the bend alignment at $V = 0$ by polymer-stabilization treatment.

The manner of variation of transmittance in the low voltage range can be used to judge whether the bend alignment is the result of the polymer stabilization.

4. EXPERIMENTAL PROCEDURE

4.1. Sample Preparation and Experiments

Sample cells were made using the liquid crystal mixture ZLI-2293, and a reactive mesogen RMM34 which is a mixture of diacrylate and monoacrylate and a small amount (5–10 wt%) of photoinitiator, all supplied by Merck Ltd. The reactive mesogen RMM34 was added to

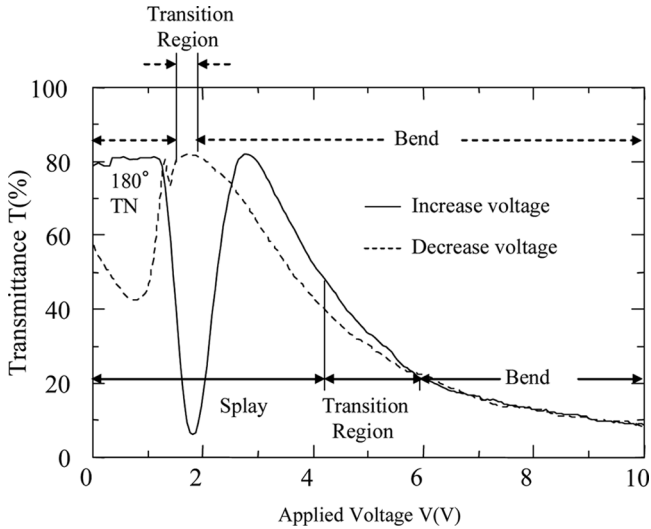

FIGURE 7 Experimental results for relationship between transmittance and applied voltage before polymer stabilization.

the nematic liquid crystal mixture ZLI-2293 at concentrations in the range of 1 to 5 wt%. The final mixture was filled into 6-μm-gap liquid crystal cells with tilted alignment produced by the parallel rubbing of polyimide coating SE-610 (Nissan Chemical Industry.) on both plates. Polymerization was induced by exposure to an ultra violet light source of approximately 0.6 mW/cm^2, centered around 365 nm (black-light) for an appropriate time. A 100 kHz sine wave voltage of 15 V was applied during exposure. The exposure time was determined so as to obtain appropriate irradiation energy density, E_{UV}, defined as the product of the irradiation power and the exposure time.

The relationship between the transmittance and the applied voltage, was measured for each sample cell. A sine wave voltage at a frequency of 1 kHz was applied. The changing rate of applied voltage was 3 V/min. Monochromatic light of wavelength 550 nm was used as the light source. The sample cell was set in a crossed Nicols. The transmission axis of polarizer was set at an angle of 45° with respect to the rubbing direction of the sample cell.

4.2. Experimental Results and Discussion

The V-T curves measured before UV light irradiation are shown in Figure 7. In this figure, the solid line indicates the V-T curve with the increase of applied voltage. It can be seen that at the initial state

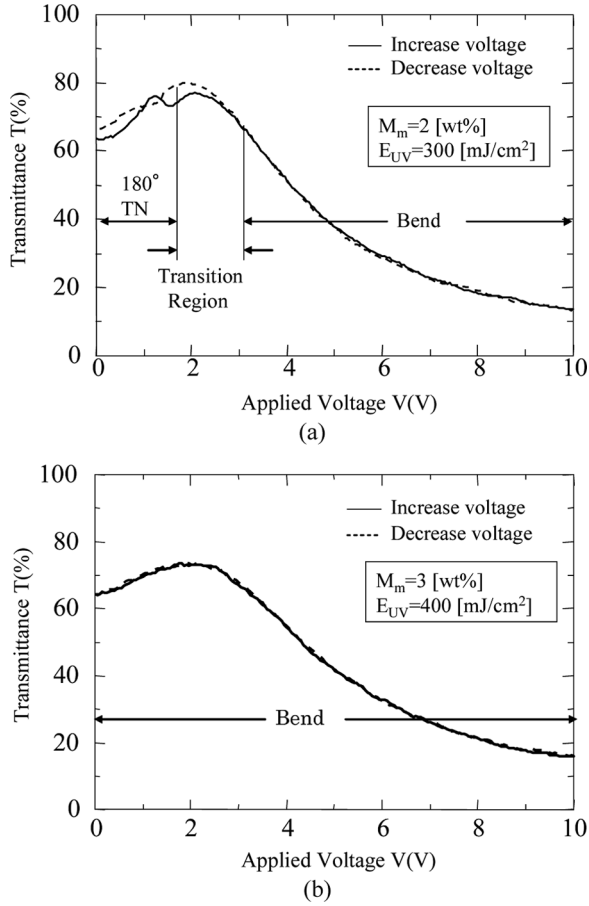

FIGURE 8 Experimental result for the relation of transmittance vs. applied voltage after polymer stabilization: (a) concentration of reactive mesogen $M_m = 2\,wt\%$ and the UV irradiation energy $E_{UV} = 300\,mJ/cm^2$, and (b) concentration of reactive mesogen $M_m = 3\,wt\%$ and the UV irradiation energy $E_{UV} = 400\,mJ/cm^2$.

of molecular alignment the configuration is in the splay alignment and the initial state is transformed to the bend state in the voltage range of 4.3 to 5.8 V. The dotted line in this figure indicates the V-T curve as the applied voltage decreases. Here it is observed that the bend state transforms into the twist state in the voltage range of 2.0 to 1.7 V. The twist state then naturally relaxes to the splay state.

Figure 8 shows the V-T curves measured for cells after being treated with the polymer-stabilizing method at the bend alignment.

Figure 8(a) represents the case with the concentration of reactive mesogen $M_m = 2\,wt\%$ and UV irradiation energy of $E_{UV} = 300\,mJ/cm^2$, and Figure 8(b) represents the case with $M_m = 3\,wt\%$ and $E_{UV} = 400\,mJ/cm^2$. In Figure 8, the states of the alignment expected for each voltage range are described. It can be seen that in the case of Figure 8(a), the twist alignment resulted from the polymer stabilization when no voltage was applied, while in the case of Figure 8(b), the bend alignment was definitively stabilized.

As mentioned, it is plausible to think that the value of A_{stab} depends on the density of polymer chains generated by photopolymerization reactions induced by UV light irradiation and on the manner of interaction between the polymer chain and liquid crystal molecules. It thought that the density of the polymer chain depends on the concentration of the reactive mesogen M_m when the UV irradiation energy E_{UV} is higher than the critical value. The UV irradiation energy E_{UV} irradiated on our sample cell exceeded the critical value. Thus, it is natural to think that the value of A_{stab} in the case of Figure 8(b) is larger than that in the case of Figure 8(a). This supports the theoretical prediction that the value of A_{stab} must be larger than the critical value A_{stabc} to definitively stabilize the bend state by polymer stabilization treatment.

5. CONCLUSIONS

Because of the introduction of an additional term which allows the explanation of the effect of polymer stabilization, it has become possible to investigate theoretically which director profile results from polymer-stabilization treatment in the nematic liquid crystal cell. As has been described in this study, the value of A_{stab} must be larger than the critical value A_{stabc} to definitively stabilize the bend alignment in the π cell. This was confirmed both theoretically and experimentally. The theoretical analysis and experimental considerations concerning the polymer-stabilization coefficient A_{stab} are left for study in the near future.

APPENDIX

In Eqs. (10), (11) and (20),

$$\begin{aligned}\frac{\partial F}{\partial n_x} - \partial_z\left(\frac{\partial F}{\partial(\partial_z n_x)}\right) = &-\{K_{33} + (K_{22} - K_{33})n_y^2\}(\partial_z^2 n_x) + (K_{22} - K_{33})n_x n_y(\partial_z^2 n_y) \\ &- K_{33} n_x (\partial_z n_x)^2 + (2K_{22} - K_{33}) n_x (\partial_z n_y)^2 \\ &- K_{22} n_y (\partial_z n_x)(\partial_z n_y) - 2K_{33} n_z (\partial_z n_y)(\partial_z n_z) \\ &+ A_{stab}(n_{stabx} n_x + n_{stab} n_y + n_{stabz} n_z) n_{stabx}, \end{aligned} \tag{A-1}$$

$$\frac{\partial F}{\partial n_y}-\partial_z\left(\frac{\partial F}{\partial(\partial_z n_y)}\right)=(K_{22}-K_{33})n_x n_y(\partial_z^2 n_x)-\{K_{33}+(K_{22}-K_{33})n_x^2\}(\partial_z^2 n_y)$$
$$-(K_{33}-2K_{22})n_y(\partial_z n_x)^2-K_{33}n_z(\partial_z n_y)(\partial_z n_z)$$
$$-2K_{22}n_x(\partial_z n_x)(\partial_z n_y)-A_{stab}(n_{stabx}n_x+n_{stab}n_y$$
$$+n_{stabz}n_z)n_{staby}, \tag{A-2}$$

$$\frac{\partial F}{\partial n_z}-\partial_z\left(\frac{\partial F}{\partial(\partial_z n_z)}\right)=-K_{11}(\partial_z^2 n_z)+K_{33}n_z\{(\partial_z n_x)^2+(\partial_z n_y)^2\}$$
$$-A_{stab}(n_{stabx}n_x+n_{stab}n_y+n_{stabz}n_z)n_{stabz},$$
$$-\frac{(\varepsilon_p-\varepsilon_n)n_z D_z^2}{\varepsilon_0\{\varepsilon_n+(\varepsilon_p-\varepsilon_n)n_z^2\}^2}. \tag{A-3}$$

Since the effective dielectric constant with respect to the z direction is $\varepsilon_0\{\varepsilon_n+(\varepsilon_p-\varepsilon_n)n_z^2\}$, D_z is related to the voltage V across the electrodes as follows

$$D_z=\frac{V}{\int_0^d \frac{1}{\varepsilon_0\{\varepsilon_n+(\varepsilon_p-\varepsilon_n)n_z^2\}}dz}, \tag{A-4}$$

In the Eqs. (13), (14), (16) and (17),

$$\frac{\partial F^S(l)}{\partial n_x(l)}=-C_{\theta l}\left\{(n_{lx}\cos\phi_l+n_{ly}\sin\phi_l)\sqrt{n_x(l)^2+n_y(l)^2+n_{lz}n_z(l)}\right\}$$
$$\times\left\{(n_{lx}\cos\phi_l+n_{ly}\sin\phi_l)n_x(l)(n_x(l)^2+n_y(l)^2)^{-\frac{1}{2}}-n_{lz}n_x(l)/n_z(l)\right\}$$
$$-C_{\phi l}\frac{n_y(l)\{n_{lx}n_x(l)+n_{ly}n_y(l)\}\{n_{lx}n_y(l)-n_{ly}n_x(l)\}}{(n_{lx}^2+n_{ly}^2)\{n_x(l)^2+n_y(l)^2\}^2}, \tag{A-5}$$

$$\frac{\partial F^S(l)}{\partial n_y(l)}=-C_{\theta l}\left\{(n_{lx}\cos\phi_l+n_{ly}\sin\phi_l)\sqrt{n_x(l)^2+n_y(l)^2}+n_{lz}n_z(l)\right\}$$
$$\times\left\{(n_{lx}\cos\phi_l+n_{ly}\sin\phi_l)n_y(l)(n_x(l)^2+n_y(l)^2)^{-\frac{1}{2}}-n_{lz}n_y(l)/n_z(l)\right\}$$
$$-C_{\phi l}\frac{n_x(l)\{n_{lx}n_x(l)+n_{ly}n_y(l)\}\{n_{ly}n_x(l)-n_{lx}n_y(l)\}}{(n_{lx}^2+n_{ly}^2)\{n_x(l)^2+n_y(l)^2\}^2}, \tag{A-6}$$

$$\frac{\partial F}{\partial(\partial_z n_x)}\Big|Z=l=\{K_{33}+(K_{22}-K_{33})n_y(l)^2\}(\partial_z n_x)\big|_{z=l}$$
$$-(K_{22}-K_{33})n_x(l)n_y(l)(\partial n_y)\big|_{z=l}, \tag{A-7}$$

$$\frac{\partial F}{\partial(\partial_z n_y)}\Big|Z = l = \{K_{33} + (K_{22} - K_{33})n_x(l)^2\}(\partial_z n_y)\Big|_{z=l} - (K_{22} - K_{33})n_x(l)n_y(l)(\partial n_x)\Big|_{z=l}. \quad \text{(A-8)}$$

REFERENCES

[1] Miyashita, T., Yamaguchi, Y., & Uchida, T. (1995). *Jpn. J. Appl. Phys.*, *34*, 177.
[2] Bos, P. L. & Rahman, J. A. 1993 SID Int. Symp. Dig. Tech. Papers, 1993, p. 273.
[3] Sueoka, K., Nakamura, H., & Taira, Y. Proc. AM-LCD & IDW, 1996, p. 133.
[4] Mori, H., Gartland, E. C. Jr., Kelly, J. R., & Bos, P. J. Proc. IDW, 1998, p. 77.
[5] Nagae, N., Miyashita, T., Uchida, T., Yamada, Y., & Ishii, Y. 2000 SID Int. Symp. Dig. Tech. Papers, 2000, p. 26.
[6] Konno, T., Miyashita, T., & Uchida, T. (1995). *ASIA DISPLAY '95*, 581.
[7] Kim, S. H. & Chien, L. C. (2004). *Jpn. J. Appl. Phys.*, *43*, 7643.
[8] Kikuchi, H., Yamamoto, H., Sato, H., Kawakita, M., Takizawa, K., & Fujikake, H. (2005). *Jpn. J. Appl. Phys.*, *44*, 981.
[9] Kossyrev, P. A., Qi, J., Priezjev, N. V., Pelcovits, R. A., & Crawford, G.-P. 2002 SID Int. Symp. Dig. Tech. Papers, 2002, p. 506.
[10] Takahashi, T., Umeda, T., Furue, H., & Kobayashi, S. (1999). *Jpn. J. Appl. Phys.*, *38*, 5991.
[11] Berreman, D. W. (1975). *J. Appl. Phys.*, *46*, 3740.